https://doi.org/10.5194/essd-2026-927
Preprint. Discussion started: 20 November 2026
© Author(s) 2026. CC BY 4.0 License.



Open Access Earth System Science Data Discussions

Development of an integrated source-profile dataset of high reactivity organic gases (HROG) for anthropogenic sources in China

Yaqin Gao[1], Hongli Wang[1]*, Rusha Yan[1]*, Sheng'ao Jing[1], Qian Wang[1], Jun Lu[1], Jingyu An[1], Yuhang Wu[1], Xinwei Feng[1], Yingge Ma[1], Dan Dan Huang[1], Yingjie Li[1], Haixia Dai[1], Qingyan Fu[1], Cheng Huang[1†]

[1]Key Laboratory of Formation and Prevention of Urban Air Pollution Complex, Ministry of Ecology and Environment; Shanghai Academy of Environmental Sciences, Shanghai, 200233, China
†Now at Shanghai Environmental Monitoring Center, State Ecologic Environmental Scientific Observation and Research Station at Dianshan Lake, Shanghai 200235, China

Correspondence to: Hongli Wang (wanghl@saes.sh.cn) and Rusha Yan (yanrs@saes.sh.cn)

Abstract.

Anthropogenic high-reactivity organic gases (HROGs) sustain the formation of ozone and secondary organic aerosol, yet the substantial variations in reactivity among HROG species lead to a potential mismatch between the mass-dominant and reactivity-dominant species, posing a challenge to current total-emission-based control strategies. Compounding this issue, source-specific characterization of critical HROG groups, particularly oxygenated and nitrogenous species, remains constrained by measurement limitations. Here, by establishing field and laboratory test platforms for major anthropogenic sources and applying advanced comprehensive measurement techniques, we develop an integrated source-profile dataset of speciated HROG emissions for five major anthropogenic source categories in China, including industrial processes, solvent use, vehicle exhausts, evaporation and residential combustion, across 45 subcategories. The reported 269 species including 75 conventional species and 194 extended species (52 hydrocarbons, 98 oxygenated and 44 nitrogenous species) were characterized under one consistent quality control conditions. The extended species account for 5.5–97.1% of the speciated source mass and 11.9–99.1% of its OH reactivity, with mean contributions above 50% for both metrics, and their inclusion substantially increases the reactivity of industrial and combustion profiles by ~90% relative to previously reported compilations. Distinct source fingerprints emerge when extended species are included. Petroleum refining and solvent-based coatings are dominated by alkanes and aromatics respectively, whereas oxygenated HROGs dominate residential combustion, diesel exhaust and particularly sources complying with the latest control requirements, such as China 6 vehicles and water-based coatings. The relative importance of extended species across diverse sectors facilitates the adjustment of speciation profiles in emission inventories. Applying the updated profiles to the 2021-based Yangtze River Delta (YRD) emission inventory alters the composition of speciated HROG emissions compared to the previously published YRD profile set, with most oxygenated species fractions increasing by far more than 0.5 times. Used in a regional model application, the updated profiles reduce the low bias of simulated formaldehyde from 39 % to 24 % and shrink the diagnosed VOC-limited area over the YRD from 25.3 % to 18.1 % of the domain, indicating that profiles missing part HROG species systematically bias diagnoses toward VOC-limited conditions. The dataset provides experimentally derived, internally consistent source profiles for emission inventories, receptor modelling and chemical transport models, and it supports a shift from mass-based to reactivity-based VOC control. Our HROG source-profile dataset can be accessed from https://doi.org/10.6084/m9.figshare.34948000 (Gao. et al., 2026).

1 Introduction

High-reactivity organic gases (HROGs) serve as critical precursors in atmospheric oxidation and therefore drive the formation of ozone (O_3) and secondary particulate matter (Heald and Kroll, 2020; Fan et al., 2024). Here we use HROG to denote the subset of

https://doi.org/10.5194/essd-2026-927
Preprint. Discussion started: 20 November 2026
© Author(s) 2026. CC BY 4.0 License.



gas-phase organic emissions with relatively large OH reaction rate constants to contribute appreciably to radical cycling and ozone formation. Operationally it comprises C1–C20 hydrocarbons, oxygenated species (OROGs, including carbonyls, alcohols, acids, furans, phenols and so on) and nitrogen/sulfur-containing species (N/S-ROGs), and it excludes the comparatively inert halocarbons that contribute to mass load but not to chemical reactivity (Gao et al., 2023; Wang et al., 2022b; Xiong et al., 2026). In China, routine ambient and emission monitoring programs primarily focus on a limited suite of Photochemical Assessment Monitoring Stations (PAMS) species and select carbonyls as proxies for the total organic burden (Ministry of Ecology and Environment of the People's Republic of China, 2018, 2014, 2019; Mo et al., 2016), leaving most of the reactive organic carbon column unresolved. However, atmospheric HROGs comprise a complex mixture of chemicals, including other non-routine measured reactive components such as furans, phenols and amines belonging to oxygenated and nitrogenous species (Gao et al., 2023). These species exhibit distinct atmospheric reactivity and secondary pollution potential (Wang et al., 2022b; Xiong et al., 2026). Notably, oxygenated species have been identified as larger contributors to radicals and ozone production in the atmosphere (Wang et al., 2022b; Lyu et al., 2024; Du et al., 2025).

In China, anthropogenic HROG emissions are primarily driven by industrial processes, transportation activities, and residential energy use, each characterized by diverse emission patterns. Over the past two decades, extensive field and experimental measurements have been performed in China to establish localized source profiles and reduce the substantial uncertainties introduced by reliance on foreign emission factors (e.g., EPA's SPECIATE database (Simon et al., 2010)). These studies have focused on subsets of HROG species as well as the full volatility-range distributions in source emissions. A Chinese source profile database built with conventional analytical techniques originally contained 56 non-methane hydrocarbons (NMHCs) and select oxygenated species (Mo et al., 2016). After compiling more than 500 domestic source profiles from published literature, the total number of unique species catalogued in the entire database was extended to 447 (Sha et al., 2021). Despite these advances, significant deficiencies remain in the measurement of HROG species beyond conventional NMHCs. First, inconsistent sampling and analytical methods across different studies may introduce additional uncertainty. Second, the coverage of quantified oxygenated species differs greatly among various anthropogenic emission sources, with the detected number ranging from 12 to 178, which limits the comparability of source profiles across categories (Sha et al., 2021). Therefore, cross-source species comparability and methodological consistency need further improvement. Latest, an emission inventory spanning the full volatility range has been developed, significantly improving secondary organic aerosol (SOA) simulations (Chang et al., 2022; Huang et al., 2023). However, the chemical pathways driving ozone formation as well as the evolution of atmospheric oxidizing capacity are considerably more complex, as they depend primarily on species reactivity rather than volatility, with reactivity varying by orders of magnitude among different compounds. Consequently, it is necessary to construct highly reactive organic gas (HROG) source profiles with targeted improvements in species coverage and methodological consistency to address the current limitations in ozone and atmospheric oxidation capacity modeling caused by these issues in existing profile databases.

This study aims to establish a consistent, measurement-derived dataset of HROG source profiles for China's major anthropogenic sources, in which every source is characterized on the same species list, with the same instruments and under one set of quality-control rules. New measurements were made for industrial processes, solvent use (including a purpose-built coating vaporization rig) and diesel vehicles; previously published measurements conducted with identical protocols were integrated for gasoline exhaust, fuel evaporation and residential combustion, and gasoline-vehicle results from the literature obtained with the same analytical approach were added for completeness. This study quantifies the contribution of the extended species to emitted mass and reactivity, documents the source-resolved fingerprints, evaluates how the profile update changes regional emission speciation relative to the previously published YRD profile set, and quantifies the consequences for simulated OROGs and for diagnosed O_3 formation regimes.

https://doi.org/10.5194/essd-2026-927
Preprint. Discussion started: 20 November 2026
© Author(s) 2026. CC BY 4.0 License.



Open Access Earth System Science Data Discussions

2 Methodology and data

2.1. Source classification

According to the Technical Guide for Compiling Integrated Emission Inventory of Air Pollutants and Greenhouse Gases (Ministry of Ecology and Environment of China, 2024) and the source-specific VOC emission inventory for the Yangtze River Delta (An et al., 2021), the compiled HROG profiles were separated into five major source categories spanning the industrial, transportation and residential sectors: industrial process, solvent use, vehicle exhaust, fuel evaporation and residential combustion. These were further divided into 45 subclasses according to process stage, material, product or fuel type. All classifications, abbreviations, identification numbers and sample counts are given in Table S1 of the Supplement.

2.2 Source sampling and testing platforms

The profile dataset was compiled using measurements from this study, our previous works and the available literature that employed the same measurement and data-treatment methods (Gao et al., 2023). New measurements with extended species coverage were conducted for industrial processes, solvent use and diesel vehicle emissions. Other source profiles for fuel evaporation and residential combustion were integrated from our previous work (Lu et al., 2025; Gao et al., 2023). Gasoline vehicle profiles were compiled from our previous work (Huang et al., 2024) and available literature (Wang et al., 2022a) to improve the completeness of the dataset. The details of experiment platforms and instrumentation are summarized in Table S2 of the Supplement and described below.

2.2.1 Industrial process sources

Field sampling was conducted at representative industrial units during 2022–2023 to quantify HROG emissions. Priority sectors included petrochemical refining, chemical manufacturing (e.g., organic chemicals, ink, rubber and pesticide), coking and wood processing. A total of 94 samples were collected using Summa canisters (Entech Inc., 3.2 L) over a 30-minute duration at standardized sampling ports located downstream of operational air-pollution treatment facilities. All treatment facilities were operating normally during sampling. The sampling method referred to HJ 732-2014 “Emission from stationary sources − Sampling of volatile organic Compounds − Bags method” and HJ 759-2023 “Ambient Air − Determination of 65 Volatile Organic Compounds − Collected in canisters and analysed by gas chromatography/mass spectrometry”.

2.2.2 Solvent use in industrial sources and coating products

Sampling at solvent-intensive industries (e.g., furniture manufacturing, packaging printing, machinery manufacturing) followed the same protocol as for industrial process sources. Because coating products volatilise over the full-service life, emissions from coating products were additionally measured on a custom-built vaporization platform.

Materials. Five coating families governed by national VOC content limits were selected: floor coatings (GB 38468-2019), architectural wall coatings (GB 18582-2020), wood coatings (GB 18581-2020), vehicle coatings (GB 24409-2020) and industrial protective coatings (GB 30981-2020). The test set comprised 43 solvent-based and 30 water-based products defined by application or binder type, obtained either directly from manufacturers or from retail outlets.

Procedure. The test methods followed GB/T 1725-2007 “Paints, varnishes and plastics − Determination of non-volatile-matter content”, GB/T 23985-2009 “Paints and varnishes − Determination of volatile organic compound (VOC) content − Difference method” and GB/T 23986.2-2023 “Paints and varnishes − Determination of volatile organic compounds (VOC) and/or semi volatile organic compounds (SVOC) content − Part 2: Gas-chromatographic method”. The custom-built vaporization system was preheated to the standard temperature of 105°C. A suction fan supplied air at 1 m s^{-1} (127 m^3 min^{-1}). A pre-weighed piece of baked aluminium foil (mass m_1) was loaded with 1–30 g (± 0.1 g) of test coating (mass m_2) and placed immediately into the heated system. The diluted sample flow (400 mL min^{-1}) was mixed with 1 L min^{-1} of nitrogen and analysed in real time by PTR-ToF-MS (channel 1) and a

https://doi.org/10.5194/essd-2026-927
Preprint. Discussion started: 20 November 2026
© Author(s) 2026. CC BY 4.0 License.



formaldehyde analyser (channel 2). In parallel, offline samples were collected in Summa canisters over 1 hour with a flow restrictor valve (InertSi®) (channel 3). Heating was stopped after 1 h and the residual mass (m_3) was weighed, giving the volatilised mass ($m_4=m_2-m_3$) used to normalise the emissions. Background samplings were conducted prior to each test with all three sampling channels. The experiments were carried out in duplicate for the majority of the coatings.

2.2.3 Vehicle exhausts

Diesel vehicle exhaust was characterized in heavy-duty chassis dynamometer tests at the Shanghai Motor Vehicle Inspection Certification & Tech Innovation Center (SMVIC). The platform comprises a chassis dynamometer (MAHA ECDM-72H, Germany) and a full-flow constant volume sampling (CVS) system (MEXA-7000 series, HORIBA). Twenty-one in-use heavy-duty vehicles (Table S3) were tested in a temperature-controlled room (25 °C), each completing two replicate runs of the China-World Transient Vehicle Cycle (C-WTVC). The fleet covered China IV, V and VI standards and five major brands. The 1800 s cycle comprises three phases approximating urban (0–900 s, ~22 km h^{-1}), rural (900–1368 s, ~42 km h^{-1}) and motorway (1368–1800 s, ~75 km h^{-1}) operation. Emissions were characterized offline by SUMMA canister sampling with GC–MS/FID and online by PTR-ToF-MS and a formaldehyde analyser. Gasoline-vehicle profiles were compiled from our own chassis dynamometer tests (Huang et al., 2024) and from the literature using online PTR-ToF-MS for China 1–6 gasoline vehicles (Wang et al., 2022a).

2.2.4 Fuel evaporation and residential combustion

Evaporative emissions from gasoline vehicles were characterized by our previous study (Lu et al., 2025). Briefly, eight light-duty gasoline vehicles covering China 3 to China 6 were tested in a variable-temperature sealed housing for evaporative determination (VT-SHED) unit for hot-soak losses (HSL) and diurnal breathing losses over 48 h, using online PTR-ToF-MS and a formaldehyde analyser together with 24 h integrated canister samples.

Residential combustion profiles were taken from Gao et al. (2023). Twenty-three samples were collected in Summa canisters at the stack outlets of household stoves operated in real households, covering four typical biomass fuels (firewood, straw, corncob and maize stalk) and two coal types (anthracite and briquette).

2.3 Comprehensive speciation based on instrumentation, data fusion and quality assurance

2.3.1 Instrument platform and species coverage

Because no single technique resolves the full reactivity-relevant range of organic gases, profiles were built by fusing four measurement channels (Figure 1): (i) offline canister samples analysed by GC–MS/FID for isomer-resolved C2–C12 hydrocarbons and C2–C6 carbonyls; (ii) H_3O^+ PTR-ToF-MS for quantification of the remaining proton-affine species, mainly oxygenated and nitrogen-containing compounds together with aromatics and PAHs; (iii) NO^+ PTR-ToF-MS for C8–C20 alkanes and selected aromatics that are either insensitive to or fragmented under H_3O^+ chemistry; and (iv) a formaldehyde analyser for HCHO. The integrated platform resolved 306 quantifiable species across the measured sources. Of these, 112 species were captured by conventional methods, including 57 PAMS species, 18 C2–C6 carbonyls, and 37 halohydrocarbons, with mean OH reaction rate constant (k_{OH}) values of 0.45 ± 0.54, 0.39 ± 0.26, and 0.04 ± 0.08 ppb^{-1} s^{-1}, respectively. The remaining 194 species belonged to the extended suite, dominated by 52 additional hydrocarbons (such as high-carbon alkanes and PAHs), 98 OROGs, and 44 N/S-ROGs, with mean k_{OH} values of 1.38 ± 1.28, 0.66 ± 0.69, and 0.47 ± 0.75 ppb^{-1} s^{-1}, respectively. Given that this study focuses on relative highly reactive components, halohydrocarbons were retained only in the final source profiles and were not discussed in detail in the main text due to their OH reactivity being approximately one order of magnitude lower than that of other groups. Finally the consolidated species list reported in the main text comprises 269 species.

Before fusion, the consistency of the channels was evaluated using the overlapping species (e.g. aromatics and carbonyls by GC–MS/FID and H_3O^+ PTR-ToF-MS and NO^+ PTR-ToF-MS). Data were merged only after their consistency was confirmed (Gao et

https://doi.org/10.5194/essd-2026-927
Preprint. Discussion started: 20 November 2026
© Author(s) 2026. CC BY 4.0 License.



al., 2023). Duplicated species were then removed according to the priority GC–MS/FID > formaldehyde analyser > H_3O^+ PTR-ToF-MS > NO^+ PTR-ToF-MS. This order preserves isomer-resolved information for the species where it exists. Where GC–MS/FID resolves only one member of an isomer family, that member is retained at its measured mixing ratio and the PTR-ToF-MS signal for the shared molecular formula is reduced by that amount, the remainder being attributed to the other isomers.

2.3.2 PTR-ToF-MS data treatment and species identification

Our PTR-ToF-MS achieves a mass resolution of 10 000, sufficient to separate isobaric ions but limited to molecular-formula identification without structural resolution. Compound assignment for each mass-to-charge ratio therefore combined the elemental-composition tool in Tofware (version 3.2.5, Tofwerk AG, Switzerland), the PTR-MS library (Pagonis et al., 2019), the PubChem database and source-specific evidence from previous studies. The elemental-composition tool generates CHONS candidates ranked by mass deviation, then the library and database select validated structures and literature evidence resolves source-specific formula identification. For residential combustion the assignments were cross-validated against two-dimensional gas chromatography time-of-flight mass spectrometry, open-path fourier transform infrared spectroscopy (Hatch et al., 2017) and NO^+ chemical ionization mass spectrometry (Koss et al., 2018). Other combustion sources referenced the same identifications. For solvent use sources, assignments were verified with a high-resolution exactive plus extended mass range mass spectrometer (Tanzer-Gruener et al., 2022), a custom-built GC (Stockwell et al., 2021) and the fuel-based inventory of vehicle emissions and volatile chemical products inventory (Coggon et al., 2021). Notably, m/z 45 (C_2H_4O), conventionally assigned to acetaldehyde, is attributed to ethylene glycol in solvent emissions (Stockwell et al., 2021; Liang et al., 2024; Tanzer-Gruener et al., 2022), and texanol (2,2,4-trimethyl-1,3-pentanediol monoisobutyrate), a latex-paint additive, is identified through its fragment ion at m/z 217 ($C_{12}H_{22}O_2H^+$) (Gkatzelis et al., 2021).

2.3.3 Quality control and quality assurance

To ensure data reliability and validity, strict quality control procedures were implemented throughout the sampling and analysis processes, covering field measurements, sample pretreatment, chemical composition analysis, method validation, and data processing. The major procedures are described as follows.

For offline sampling pretreatment, each canister was repeatedly purged with high-purity nitrogen under heated conditions using an automatic cleaning system (JHX-2000, Wuhan Juhexin Environmental Protection Technology Co., Ltd.). After cleaning, the canisters were evacuated to a vacuum state (termination pressure 50–150 mTorr) and rechecked with a pressure gauge before sampling to verify maintenance of the vacuum condition. During offline sampling, PTFE filters were installed upstream of the canister to remove particulate matters.

After collection, the canister samples were analyzed by a GC−MS (Agilent 7890A−5975C) and PTR-ToF-MS (Tofwerk, VOCUS2R) within 7 days. Each analytical day, one PAMS (Photochemical Assessment Monitoring Station) standard gas with a mixing ratio of 2 ppb and one nitrogen blank were analyzed daily, with a deviation of ≤10% for the standard and below the method detection limit for the blank.

PTR-ToF-MS instruments were calibrated against multi-component standard mixtures before measurements. Species without authentic standards were quantified from the ion–molecule reaction kinetics using the transmission- and k-rate-based approach, which typically carries larger uncertainty (~50%) than direct calibration (~10%) (Gao et al., 2023; Sekimoto et al., 2017). Coating and vehicle tests were replicated, with background subtraction performed.

2.4 Air quality model configuration

Air quality simulations were conducted with the Community Multiscale Air Quality model (CMAQ, version 5.3.2) using the SAPRC07tc chemical mechanism. Three-domain setup (36 km, 12 km, 4 km) in this study enables refined spatial characterization of the O_3–NOx–VOC sensitivity over the YRD. Meteorological fields were generated by the Weather Research and Forecasting

https://doi.org/10.5194/essd-2026-927
Preprint. Discussion started: 20 November 2026
© Author(s) 2026. CC BY 4.0 License.



model (WRF, version 3.9.1). Anthropogenic emissions combined the MIX inventory for eastern Asia (Li et al., 2017b), the Multi-resolution Emission Inventory for China (MEIC, http://www.meicmodel.org/) (Li et al., 2017a; Zheng et al., 2018), and a local high-resolution emission inventory for the YRD region (An et al., 2021) to better reflect the most recent anthropogenic activities in this region. Biogenic emissions were calculated online using MEGAN v3.1 (Guenther et al., 2012). Remaining model settings, including physical parameterizations, initial and boundary conditions, and chemical transport, followed Yan et al. (2024).

Two parallel scenarios were designed to quantify how updated source speciation profiles affect simulations of key ROG species and ozone sensitivity regime classification. The New-simulated scenario adopted the updated emission speciation profiles in this study, while the Base-simulated scenario retained the original YRD profiles (An et al., 2021) with all other model configurations unchanged. Given that emission estimates were primarily derived using the emission factor method, we scaled up the emissions in the New-simulated scenario based on the ratio of the expanded species to the traditional components. Simulations spanned 16 July to 17 August 2024. Hourly outputs from the 4 km modelling domain were extracted and validated against concurrent Shanghai ROG observations. The scenario differences isolate the effects of emission profiles updates on the simulated concentrations of key ROG species and the diagnosed ozone formation sensitivity regimes.

The ozone formation sensitivity regimes were classified using the formaldehyde-to-nitrogen dioxide ($HCHO/NO_2$) ratio. Grid cells defined as VOC-limited ($HCHO/NO_2 < 0.81$), transitional ($0.81 \leq HCHO/NO_2 \leq 1.35$), and NO_x-limited ($HCHO/NO_2 > 1.35$). This YRD-localized threshold range established by Li et al. (2022b) achieves an overall accuracy exceeding 92% by matching indicator-based regimes with actual O_3 responses to precursor perturbations, which is more reliable and effectively reduces classification uncertainties in the target region.

3 Results and discussion

3.1 Contribution of the extended species to mass and reactivity

Across all source categories the extended species (52 hydrocarbons, 98 OROG species and 44 N/S-ROG species) contribute between 5.5% (VEIII) to 97.1% (SWW) of the speciated mass and between 11.9% (VEIII) to 99.1% (SWA) of the OH reactivity, with average contributions above 50% for both metrics. The spread is itself informative. Sources dominated by light hydrocarbons that are already well covered by traditional GC MS/FID methods (e.g. gasoline-vehicle evaporative emissions) show the smallest extension. Whereas sources whose reactivity resides in the extended OROG and N/S-ROG species, such as water-based coatings and diesel vehicle exhaust, show the largest extension, and for these sources the extension frequently exceeds the mass covered by the conventional species list. Because the extended species are characterized by higher reactivity than the conventional reactive species (average reactivity 0.439 ppb^{-1} s^{-1} for conventional species and 0.807 ppb^{-1} s^{-1} for extended species; Figure 1), their contribution to reactivity systematically exceeds their contribution to mass.

3.2 Source-resolved chemical fingerprints

The distinct speciation profiles described above translate into marked compositional heterogeneity across source categories (Figure 2). Industrial sources showed the most complex composition, with chemical fingerprints strongly dictated by specific process steps. In petroleum refining, bulk loading was characterized by PAMS ≤C12 alkanes (40.7%), whereas waste treatment displayed a dual distribution of ≤C12 (28.4%) and high-carbon alkanes (18.0%). For organic chemical sources, acids/esters were the predominant group (25.8%), surging to 71.4% in ink production. Other industrial processes showed distinct markers: oxygenated aromatics in rubber products (30.6%); aromatics in pesticide (26.0%), coke (42.2%), and fertilizer/urea production (63.0%); N/S-ROGs in fertilizer/synthetic ammonia (47.0%); and carbonyls (43.4%) in plywood manufacturing.

Solvent use sources, conversely, reflected clear formulation-driven patterns. Our chamber measurements confirmed that aromatic hydrocarbons predominated in solvent-based coatings, particularly in floor and industrial protective coatings (49.3–87.9%), while acids/esters dominated in solvent-based wood (46.2%) and vehicle coatings (54.1%). These profiles converged well with our real-

https://doi.org/10.5194/essd-2026-927
Preprint. Discussion started: 20 November 2026
© Author(s) 2026. CC BY 4.0 License.



world sampling results in furniture (acids/esters, 50.2%) and machinery manufacturing (acids/esters, 25.8%; aromatics, 22.4%), lending confidence to the representativeness of our source signatures. In contrast, water-based coatings were primarily characterized by alcohols/ethers in industrial protective, vehicle, and wall coatings (31.4%–45.7%), whereas oxygenated aromatics dominated in water-based floor (32.0%) and wood coatings (25.7%). Notably, our real-world sampling revealed that alcohols/ethers also dominated in packaging printing (26.1%)—a signature more characteristic of water-based coatings (avg. 33.1%) than solvent-based ones (8.5%) based on our chamber measurements. This consistency underscores the diagnostic value of alcohol/ether signatures for distinguishing water-based solvent contributions in source apportionment.

Transportation sources demonstrated distinct fuel-dependent fingerprints. Gasoline vehicle exhaust was characterized by a mix of alcohols/ethers (24.4%–57.0%), aromatics (11.5%–27.6%), and alkanes (10.7%–24.9%), followed by carbonyls (4.3%–9.1%) and alkenes (3.9%–8.1%). In contrast, evaporative emissions from gasoline vehicles were heavily skewed towards alkanes (32.4%–61.7%). Diesel vehicle emissions presented a different profile, dominated by acids/esters (29.8%–38.5%), N/S-ROGs (14.0%–24.7%), and high-carbon alkanes (6.8%–9.0%). With tightening standards from China III to China VI, the hydrocarbon fraction of gasoline exhaust decreases from 58.4% to 28.2% while the oxygenated fraction increases from 37.3% to 67.4%, indicating that hydrocarbon-mass reductions are accompanied by a compositional shift that amplifies the relative importance of chemically reactive oxygenated species.

Residential combustion sources also diverged markedly based on fuel type. Biomass burning was the primary source of carbonyls (36.9%; range: 28.5%–38.9%) and alkenes (21.0%; range: 13.8%–35.7%). Conversely, residential coal combustion was characterized by lower carbonyls (26.8%) but elevated furans (26.5%), C2–C21 alkanes (12.5%) and oxygenated aromatics (9.8%). Although polycyclic aromatic hydrocarbons (PAHs) constituted only a minor fraction (5.6%) in coal combustion, this proportion was distinctly higher than in any other source category (max. 1.6%). The PAHs as well as high-carbon alkanes, furan and phenols in the coal profiles are consistent with pyrolysis of the coal macromolecular structure and incomplete combustion (Gao et al., 2023).

A further regularity emerges for sources that comply with recent control requirements. China 6 vehicles and water-based paints emit OROG-dominated mixtures because these technologies remove or replace the hydrocarbon solvents that historically dominated the profiles. Although high-reactivity hydrocarbons are increasingly replaced, the potentially high reactivity of OROG warrants continued attention, as the reactivity benefit of VOC mass reduction may not scale linearly with mass removal.

3.3 Enhanced unit reactivity and comparative significance

As shown in Figure 3, OH reactivity normalized to HROG mass varied substantially across source categories. Residential combustion displayed the highest unit reactivity, with coal combustion reaching 0.20 s^{-1}, markedly exceeding other sources and underscoring the strong chemical potency of its emissions. Industrial process sources ranked next, among which wood processing (0.18 s^{-1}) and petroleum refining (0.15 s^{-1}) showed particularly high values, suggesting that even relatively low emission masses from these sectors can generate disproportionately large atmospheric chemical impacts. Furthermore, the reactivity of gasoline vehicle evaporative emissions (0.09–0.18 s^{-1}) remained substantial. In contrast, solvent-based coatings and diesel/gasoline vehicle exhausts generally displayed lower unit reactivities, typically ranging from 0.05 s^{-1} to 0.13 s^{-1}, with solvent-based wood coatings and China V-standard diesel vehicles showing the lowest values.

Compared with the most recent integrated compilation, which was assembled from >500 previously published profiles (Sha et al., 2021), the unit reactivities derived in this study were still systematically higher. The increases were most pronounced for biomass combustion and industrial process sources, whose reactivities were approximately 1.9 times those reported previously, while solvent use and mobile sources were about 1.2 times higher than literature benchmarks. This elevation is primarily attributable to the further extended coverage of HROG species in this study. Coal and biomass combustion were characterized by furans and alkenes, whereas specific industrial sources, such as organic chemical production and rubber products, were associated with distinctive emissions of N/S-containing reactive organic gases and oxygenated aromatics, respectively. For mobile sources, the reactivity profile was strongly shaped by fuel type and emission standards. Alkenes accounted for 42.9% of the total reactivity of gasoline vehicles

https://doi.org/10.5194/essd-2026-927
Preprint. Discussion started: 20 November 2026
© Author(s) 2026. CC BY 4.0 License.



exhausts, rising to 75.2% in evaporative emissions of gasoline vehicles. Notably, under the stricter China VI emission standards, the contribution of oxygenated reactive organic gases increased from 22.9% to more than 50.9%, with a similar rise observed in gasoline evaporative emissions (4.1% to 29.2%). Moreover, oxygenated ROGs (mainly carbonyls and furans) together accounted for over 45% of the reactivity in diesel vehicle emissions, highlighting an evolving chemical signature of transportation-related sources.

3.4 Comparison with the YRD inventory

To address how the profile update changes regional emission speciation, the profiles from this study and the YRD inventory (An et al., 2021) were applied to the same activity data, thereby isolating the effect of speciation in the differences reported here. To ensure comparability with previous inventories that grouped HROG by carbon bonds and reactivity for ozone formation mechanisms and computational efficiency, this study aggregated measured species according to the SAPRC07 mechanism framework (Carter, 2010). Figure 4 compares the resulting SAPRC07-speciated organic gas emissions for the industry, residential, and transportation sectors. The right axis expresses the ratio of the species fraction in this study to that in the YRD inventory on a logarithmic scale, with the dashed line denoting parity (ratio = 1). For at least one third of the 42 SAPRC07 species in each sector (11–14 species) the two speciations agreed within a factor of 0.5–1.5. Nevertheless, pronounced and systematic deviations emerged for several chemical classes, and the direction of these deviations differed among the sectors. For species that were absent from, or negligible in, the YRD speciation (fractions below 0.001%), including BALD, GLY, MGLY, BACL, IPRD, FACD and AACD, the plotted ratios represent lower bounds rather than exact values.

The updated speciation reveals a systematic shift toward more reactive OVOC and alkenes, especially in the industrial and transportation sectors, whereas the residential sector shows a pronounced reassignment from aromatics to alkanes and carbonyls. In the industry sector, the OVOC fraction is 1.8 times that of the YRD inventory (31.7% vs. 17.4%). Specifically, BACL, BALD, AACD, and IPRD are elevated by more than 500-fold; FACD, GLY, MGLY, PRD2, and CRES by more than 20-fold; and ACRO, HCHO, and CCHO by more than 50%. Selected ALKENE, ALK, and ARO (OLE2, ALK3, ALK5, and ARO1) also show enhancements ranging from 50% to 1.5-fold.

These shifts are largely driven by emissions from industrial solvent use (e.g., coatings, inks, printing, and furniture manufacturing), chemical production (such as phenol-formaldehyde resins), and coking processes in the YRD region. The concurrent increase in the ALK class likely reflects the historical omission of species such as branched alkanes, alkyl ketones, and alkyl esters in previous profiles. In short, the relative changes can also be attributed to the expanded OVOC coverage. Crucially, these results highlight the limitations of coarse lumping mechanisms for OVOC; such oversimplification can lead to significant biases in investigating ozone formation mechanisms.

In the transportation sector, the OVOC share increases fivefold (23.2% vs. 4.7%) and the alkene fraction nearly doubles (14.9% vs. 7.6%). These increases are driven mainly by CRES, AACD, and MEOH, which are elevated by more than 500-fold, and by HCHO, BACL, and ETOH, which are elevated by more than 20-fold. Other OVOC species (MGLY, FACD, PRD2, and CCHO) and alkenes (APIN, 13BDE, ISOP, ETHE, and ACYE) also increase by more than 0.5-fold. These shifts reflect the broader coverage of HROGs in the measurements used here, whereas the YRD profiles tended to allocate the corresponding mass to aromatics and light alkenes.

More importantly, these are not minor redistributions among chemically similar species; they directly affect the estimated reactivity of emissions. The enhanced OVOC and alkene fractions in the industrial and transportation sectors increase radical sources and raise ozone formation potential, while the reduced aromatic share in the residential and industrial sectors lowers the estimated SOA formation potential relative to the YRD inventory. Accurately representing these high-reactivity species is therefore essential for constraining ozone production regimes and evaluating control strategies in the YRD region.

https://doi.org/10.5194/essd-2026-927
Preprint. Discussion started: 20 November 2026
© Author(s) 2026. CC BY 4.0 License.



3.5 Updated profiles improved simulated OVOC concentrations

Simulated concentrations of OVOCs can be used to evaluate the performance of emission speciation profiles in air quality modeling, and HCHO in particular serves as the key indicator species in ozone sensitivity regime classification. Figure 5 compares the observed and simulated diurnal variations of HCHO, CCHO, and total OVOCs at the Shanghai Supersite when the model was driven with the original and updated speciation profiles. In the Base-simulated scenario, the ratios of simulated versus observed ($R_{S/O}$) period-mean concentrations were 0.61, 0.57, and 0.67 for HCHO, CCHO, and total OVOCs, respectively, indicating that the original profiles underestimated the abundance of these oxygenated species by 33–43%, similar to the OVOC low biases reported in previous modeling studies over eastern China (Li et al., 2022a).

In comparison, when the updated speciation profiles were applied (the New-simulated scenario), the simulated concentrations aligned more closely with the observations for HCHO ($R_{S/O}$ = 0.76), CCHO ($R_{S/O}$ = 0.65) and total OVOCs ($R_{S/O}$ = 0.79) in terms of diurnal variation and magnitude (Figure 5 a–c). This update reduced the HCHO underestimation from 39% to 24% (Figure 5 a), lending confidence to the HCHO/NO_2 ratios and hence to the regime patterns derived from the New-simulated scenario. For the total OVOCs (Figure 5 c), the simulations were generally within the observed variability at night and in the early morning, but a residual underestimation persisted especially around midday and during the afternoon. The temporal correlations were similar in the two simulations (r = 0.83 versus 0.81 for HCHO, 0.38 versus 0.37 for CCHO, and 0.72 versus 0.70 for total OVOCs), indicating that the updated profiles mainly corrected the magnitude rather than the diurnal phasing of OVOCs. In addition to the insufficient representation of secondary formation of oxygenated VOCs in the model, recent studies have shown that meteorology-dependent emissions, particularly the temperature dependence of biogenic and evaporative VOC emissions, are subject to considerable uncertainty and exert their strongest influence during daytime hours (Qin et al., 2025). These aspects are beyond the scope of the present study, which focuses on emission speciation profiles, and will be explored in future work.

3.6 Implications for diagnosed O_3 sensitivity regimes

The spatial distributions of O_3 sensitivity regimes over the YRD in summer 2024, diagnosed from the period-mean HCHO/NO_2 ratios with the localized thresholds of Li et al. (2022b), are presented in Figure 6. For the New simulation with updated speciation profiles, the NOx-limited and transitional regimes together account for more than 80 % of the domain (47.2 % and 34.6 %, respectively), while the VOC-limited regime accounts for only 18.1 %, indicating that the YRD is approaching the cross-over stage of O_3–NOx–VOC sensitivity transition. Spatially, the VOC-limited regime is concentrated in highly urbanized and industrialized areas, including the Shanghai metropolitan area, the southern Jiangsu city cluster along the Yangtze River, and the Hangzhou Bay coastal region. The transitional regime forms a belt surrounding these urban cores and the Yangtze River, whereas the NO_x-limited regime is widely distributed over less urbanized and less industrialized areas in central and western Anhui and southern Zhejiang.

Notably, the diagnosed regime pattern proved sensitive to the source speciation profiles. When the previous profiles were applied (Base-simulated scenario), the VOC-limited area expanded substantially (Figure 6) from 18.1% to 25.3%, with the most pronounced enlargement along the central Jiangsu coast and over the Shanghai metropolitan area, whereas the NO_x-limited and transitional regimes contract correspondingly. This occurs because the outdated profiles underestimate HROG emissions such as OVOCs, leading to a lower simulated HCHO/NO_2 ratio and biasing the diagnosed regimes toward VOC-limited conditions. Given that the updated profiles better represent the current YRD emission characteristics and yield OVOC simulations that are more consistent with observation, the New-simulated regime is considered more representative.

This change in regime distribution is not a simple numerical rescaling of the indicator, but reflects changes in radical chemistry. Our separate modeling study based on the updated profiles (Li et al., 2026) shows that the updated speciation increases the OVOC share of anthropogenic VOC emissions to 56.9%, 44.6% and 39.2% for diesel vehicles, residential biomass burning, and industrial processes, respectively, with aldehyde contributions nearly doubled and a particularly large increase in HCHO. Mechanistically, OVOC photolysis accounts for 90%–98% of primary HO_2 production in urban areas of the YRD, with primary OVOCs alone contributing 20%–50%, while the HO_2 + NO pathway sustains 53%–63% of the daytime O_3 production rate at the Shanghai supersite.

https://doi.org/10.5194/essd-2026-927
Preprint. Discussion started: 20 November 2026
© Author(s) 2026. CC BY 4.0 License.



Primary OVOCs therefore act both as proxy species entering the indicator and as direct sources of radicals that determine the local NOx–VOC balance. Underestimation of primary OVOCs in the outdated profiles suppresses both simulated HCHO and radical supply, so that the reduction of the VOC-limited area from 25.3 % to 18.1 % essentially reflects a genuine enhancement of VOC reactivity relative to NOx.

These findings have clear implications for control strategy. The coexistence of the three regimes within YRD region implies that no single control strategy can be uniformly effective. In the urban cores that remain VOC-limited (e.g., Shanghai and the southern Jiangsu areas), continued VOC emission reductions remain the prerequisite for O_3 abatement, whereas NOx reductions alone would be inefficient or even counterproductive. In contrast, over nearly half of the domain that is already NOx-limited, further NOx controls directly reduce regional O_3. Accordingly, the YRD should adopt a spatially differentiated strategy of "city-scale VOC-first, region-scale NO_x-synergistic" control. Moreover, the VOC-first priority should not be limited to traditional non-methane hydrocarbons, but should explicitly include HROG, especially primary OVOCs, which remain largely absent from current control inventories and have substantially higher ozone formation efficiency per unit mass than most traditional precursors.

3.7 Outlook

The extended ROG-speciation source profiles developed in this study could be integrated into source apportionment and emission inventory studies, serve as fundamental input parameters for atmospheric chemistry transport models (e.g., WRF-CMAQ) and enable quantitative evaluations of spatial distributions for specific chemical components. Based on field measurements under the same quality control condition, this dataset provides local and comprehensive measurement data and significantly reduces uncertainties associated with various methodologies in existing studies.

By combining established frameworks like MEIC and atmospheric chemistry transport models, these speciated profiles provide unprecedented resolution for resolving source-specific chemical fingerprints, improving model representation of ROG-driven atmospheric processes, and identifying previously unquantified environmental impacts from extended ROG species emissions. Moreover, through bridge the dataset and modeling, the dataset could facilitate the evolution of air quality policies from mass-based regulation to reactivity-driven control strategies. This work establishes a critical foundation for advancing atmospheric chemistry research and evidence-based air quality management in China.

4 Data availability

The integrated source-profile dataset of high reactivity organic gases (HROG) for anthropogenic sources in China can be accessed from https://doi.org/10.6084/m9.figshare.34948000 (Gao. et al., 2026). It includes three worksheets: (1) profile — Species-resolved source profiles in mass-fraction units. Each source group is represented by the mean profile (avg) and its standard deviation (stdev) across samples; the mean mass fractions of each group sum to 1. Source groups are organized in a four-level hierarchical header. (2) profile OH reactivity — Species-specific OH reactivity contributions (species mass fraction × k_{OH}) for each source profile, with the total OH reactivity of each source group provided in the summary row. This enables assessment of the relative ozone- relevance of individual species and sources. (3) Statistics — Mass profiles aggregated from the 269 HROG species into the 18 HROG chemical classes for each source group (halocarbons excluded), facilitating direct comparison of chemical compositions across sectors and with emission inventories and chemical transport models.

5 Conclusions and implication

An integrated dataset of speciated HROG source profiles for five key categories of Chinese anthropogenic sources, including industrial processes, solvent use, vehicle exhaust, evaporation and residential combustion, has been developed. Built on one consistent measurement platform and quality-control protocol, the dataset reports 269 HROG species (75 conventional and 194 extended species, the latter dominated by long-chain hydrocarbons and O/N/S-ROGs. The extended species contribute on average

https://doi.org/10.5194/essd-2026-927
Preprint. Discussion started: 20 November 2026
© Author(s) 2026. CC BY 4.0 License.



more than half of both emitted mass and OH reactivity, and up to 97 % and 98 %, respectively, for individual sources, with their reactivity contribution systematically exceeding their mass contribution. Distinct source fingerprints are documented: alkanes and aromatics dominate petrochemical processing and solvent use, whereas oxygenated HROGs dominate residential combustion and diesel exhaust and become increasingly dominant as sources comply with the most recent control requirements (China 6 vehicles and water-based coatings). Replacing the previously published YRD profiles with the updated ones changes regional emission speciation substantially while using identical activity data, by increasing the mass fraction attributed to oxygenated mechanism species for mobile and industrial sources; when implemented in WRF–CMAQ, the updated profiles reduce the formaldehyde low bias from 39 % to 24 % and reduce the diagnosed VOC-limited area over the YRD from 25.3 % to 18.1 %, indicating that outdated profiles bias the diagnosed O_3 formation regime toward VOC-limited conditions. These results support a transition from mass-based to reactivity-based VOC control and argue for including primary OVOCs explicitly in VOC control inventories.

Financial support.

This research has been supported by the National Key Research and Development Program of China (Grant No. 2023YFC3706105), Jing-Jin-Ji Regional Integrated Environmental Improvement-National Science and Technology Major Project (2026ZD1209000), and the Shanghai Rising-Star Program (24YF2736300).

Author contribution.

YG, HW, RY designed the study; YG developed the dataset; RY conducted regional model validation and applications; SJ, QW, JL, YW, XF, YM, DDH, YL contributed to source sampling, instrumental analysis and source-specific data analysis; YG wrote the original draft; HD, QF, and CH contributed to manuscript revision.

Competing interests

The contact author has declared that none of the authors has any competing interests.

https://doi.org/10.5194/essd-2026-927
Preprint. Discussion started: 20 November 2026
© Author(s) 2026. CC BY 4.0 License.

Figures.

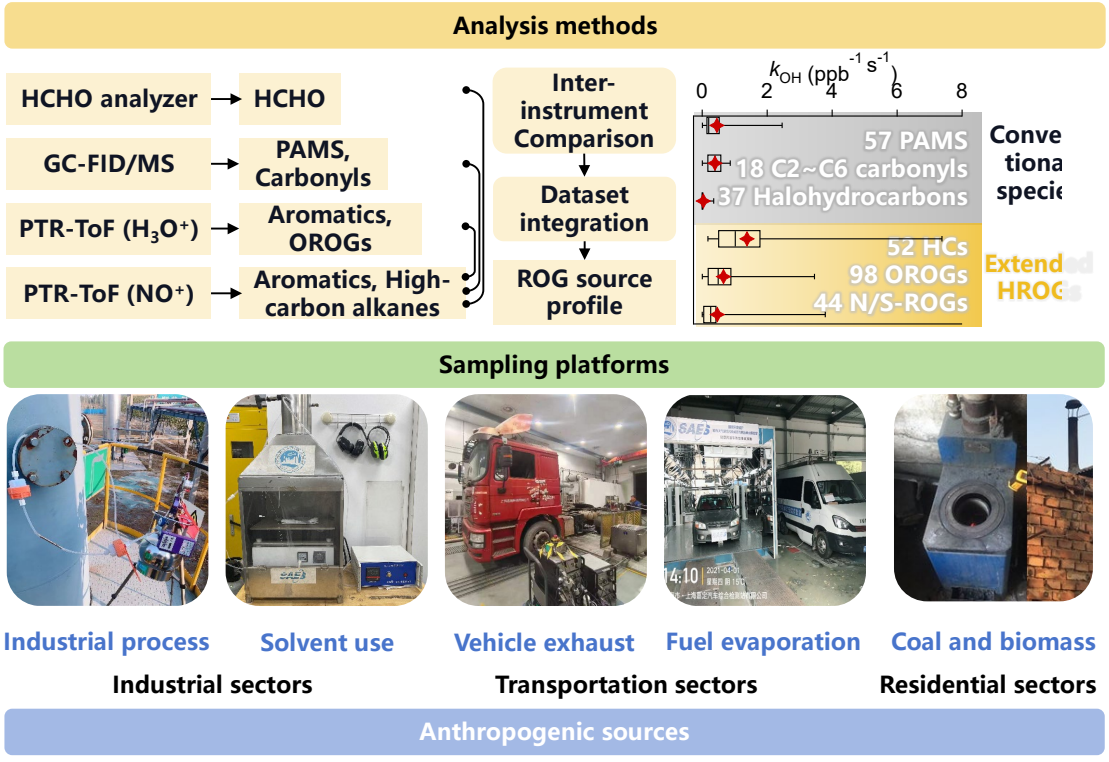


Figure 1. Framework for constructing the extended HROG speciation dataset for typical anthropogenic sources: source categories, sampling platforms, analytical methods, and chemical composition.

425

https://doi.org/10.5194/essd-2026-927
Preprint. Discussion started: 20 November 2026
© Author(s) 2026. CC BY 4.0 License.

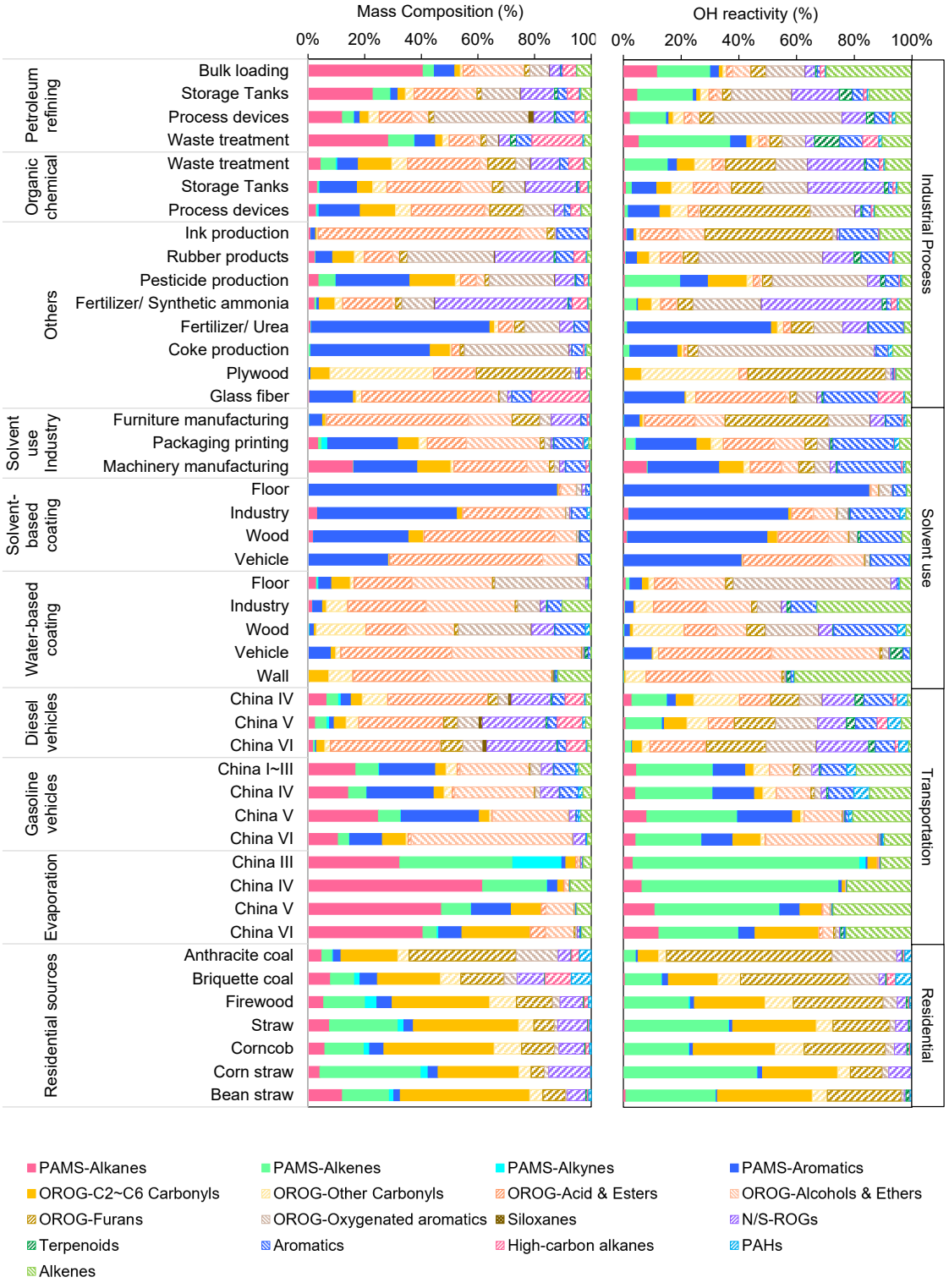


Figure 2. Compositions of mass and OH reactivity for HROG groups emitted from industrial process, solvent use, transportation and residential combustion sources.

https://doi.org/10.5194/essd-2026-927
Preprint. Discussion started: 20 November 2026
© Author(s) 2026. CC BY 4.0 License.

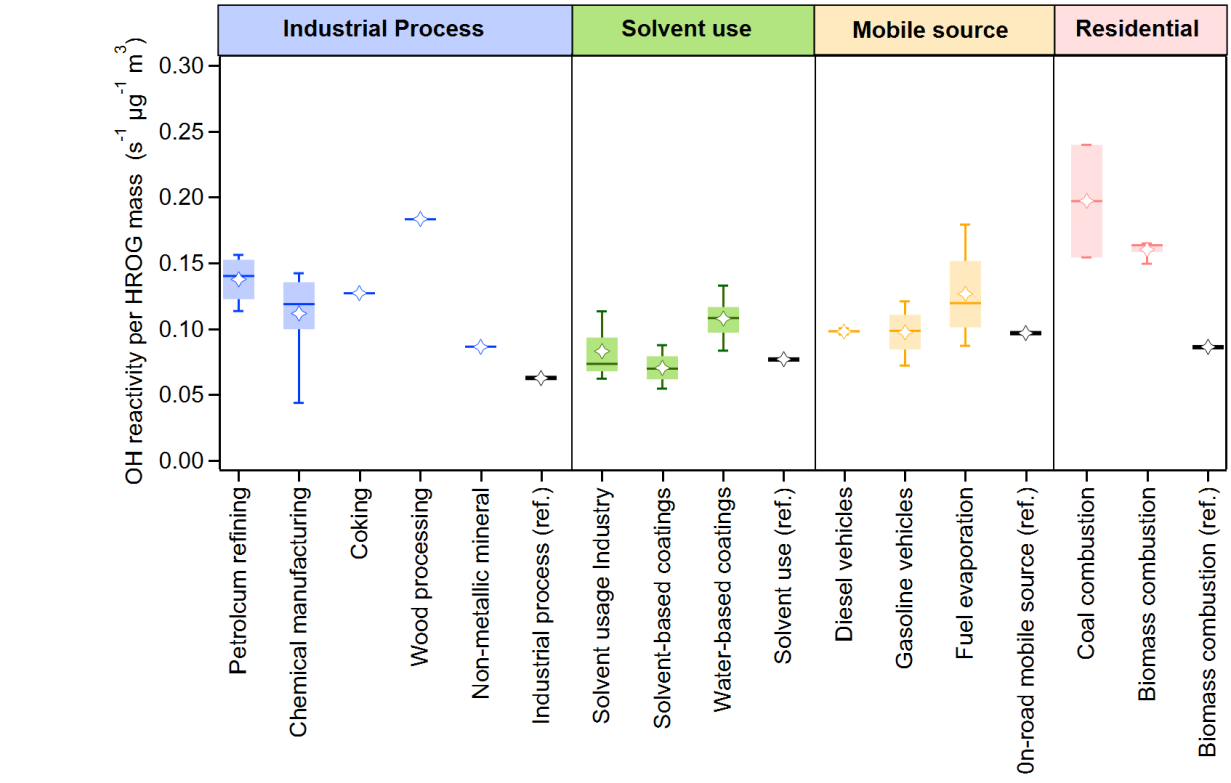


Figure 3. Comparison of OH reactivity per unit ROG mass among anthropogenic sources between this study and the previous compilation (Sha et al., 2021).

https://doi.org/10.5194/essd-2026-927
Preprint. Discussion started: 20 November 2026
© Author(s) 2026. CC BY 4.0 License.

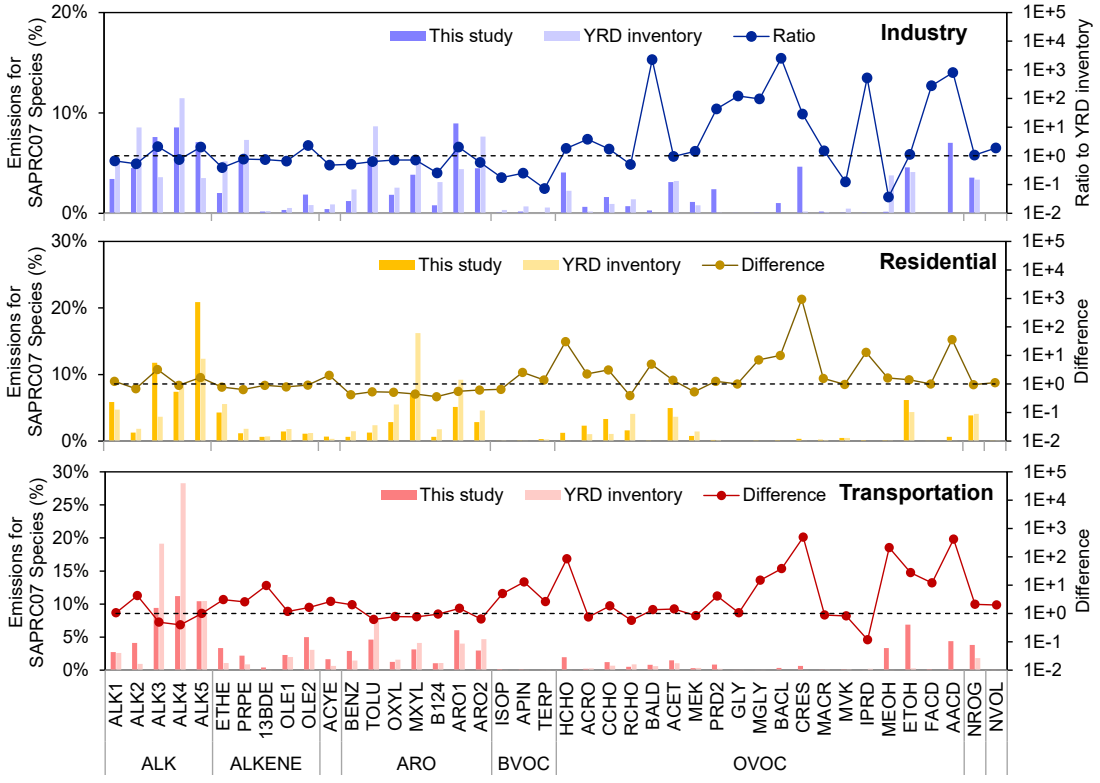


Figure 4. SAPRC07 mechanism-species comparison of YRD emissions derived with the updated (this study) and previous profile, by source sector: share (%) and share difference (the ratio of the mass fraction relative to YRD emissions).

https://doi.org/10.5194/essd-2026-927
Preprint. Discussion started: 20 November 2026
© Author(s) 2026. CC BY 4.0 License.

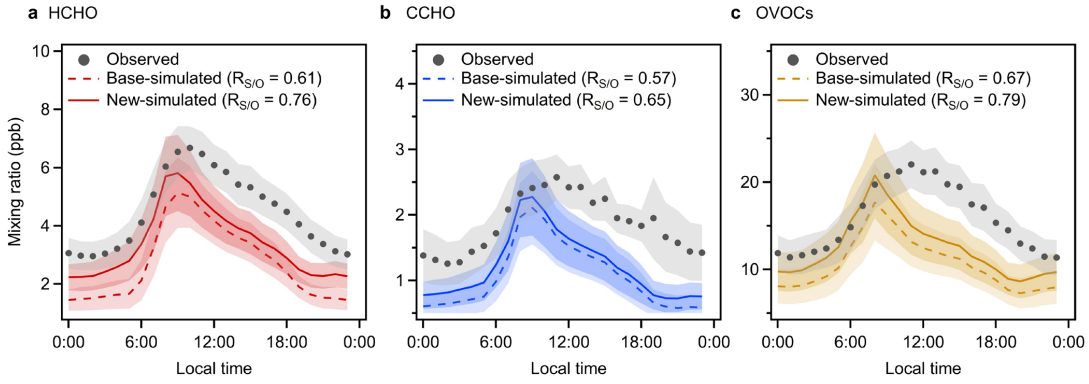


Figure 5. Diurnal variations of observed and simulated (a) HCHO (formaldehyde), (b) CCHO (acetaldehyde), and (c) total OVOCs at the Shanghai Supersite (SAES) during 16 July–17 August 2024. The dots denote the period-mean diurnal profiles of the observed concentrations, and the dashed and solid lines denote the Base- and New-simulated concentrations; shaded areas indicate one-third standard deviations. Insets report the ratio of simulated to observed mean concentrations ($R_{S/O}$).

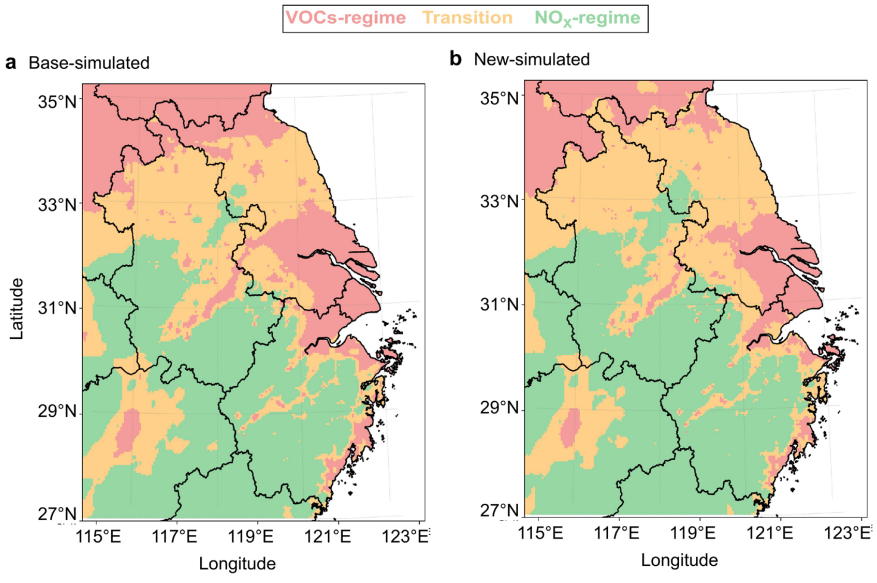


Figure 6. Spatial distributions of the O_3 formation sensitivity regimes over the YRD in summer 2024 in (a) Base-simulated and (b) New-simulated scenario, respectively, diagnosed from the period-mean HCHO/NO_2 ratios with the localized thresholds of Li et al. (2022b). VOCs-regime: HCHO/NO_2 < 0.81; Transition: 0.81 ≤ HCHO/NO_2 ≤ 1.35; NOx-regime: HCHO/NO_2 > 1.35.

https://doi.org/10.5194/essd-2026-927
Preprint. Discussion started: 20 November 2026
© Author(s) 2026. CC BY 4.0 License.



References

An, J., Huang, Y., Huang, C., Wang, X., Yan, R., Wang, Q., Wang, H., Jing, S. a., Zhang, Y., Liu, Y., Chen, Y., Xu, C., Qiao, L., Zhou, M., Zhu, S., Hu, Q., Lu, J., and Chen, C.: Emission inventory of air pollutants and chemical speciation for specific anthropogenic sources based on local measurements in the Yangtze River Delta region, China, Atmos. Chem. Phys., 21, 2003-2025, 10.5194/acp-21-2003-2021, 2021.

Carter, W. P. L.: Development of the SAPRC-07 chemical mechanism, Atmos. Environ., 44, 5324-5335, https://doi.org/10.1016/j.atmosenv.2010.01.026, 2010.

Chang, X., Zhao, B., Zheng, H., Wang, S., Cai, S., Guo, F., Gui, P., Huang, G., Wu, D., Han, L., Xing, J., Man, H., Hu, R., Liang, C., Xu, Q., Qiu, X., Ding, D., Liu, K., Han, R., Robinson, A. L., and Donahue, N. M.: Full-volatility emission framework corrects missing and underestimated secondary organic aerosol sources, One Earth, 5, 403-412, 10.1016/j.oneear.2022.03.015, 2022.

Coggon, M. M., Gkatzelis, G. I., McDonald, B. C., Gilman, J. B., Schwantes, R. H., Abuhassan, N., Aikin, K. C., Arend, M. F., Berkoff, T. A., Brown, S. S., Campos, T. L., Dickerson, R. R., Gronoff, G., Hurley, J. F., Isaacman-VanWertz, G., Koss, A. R., Li, M., McKeen, S. A., Moshary, F., Peischl, J., Pospisilova, V., Ren, X., Wilson, A., Wu, Y., Trainer, M., and Warneke, C.: Volatile chemical product emissions enhance ozone and modulate urban chemistry, Proceedings of the National Academy of Sciences, 118, e2026653118, doi:10.1073/pnas.2026653118, 2021.

Du, C., Wang, H., Gao, Y., Yan, R., Jing, S. a., Zhou, M., Wang, Q., Lou, S., Huang, C., Huang, D. D., Shang, Y., and An, J.: Processes Driving Diurnal and Seasonal Variations of Formaldehyde in an Urban Environment, ACS Earth and Space Chemistry, 10.1021/acsearthspacechem.5c00020, 2025.

Fan, Y., Song, Z., Wu, Y., Ren, X., Bi, C., Ye, W., Wei, H., and Xu, Y.: Chemicals of Emerging Concern in Water-Based Paint Products, Environmental Science & Technology Letters, 10.1021/acs.estlett.4c00052, 2024.

Gao, Y., Wang, H., Yuan, L., Jing, S., Yuan, B., Shen, G., Zhu, L., Koss, A., Li, Y., Wang, Q., Huang, D. D., Zhu, S., Tao, S., Lou, S., and Huang, C.: Measurement report: Underestimated reactive organic gases from residential combustion – insights from a near-complete speciation, Atmos. Chem. Phys., 23, 6633-6646, 10.5194/acp-23-6633-2023, 2023.

Gao., Y., Wang., H., Yan., R., Jing., S., Wang., Q., Lu., J., An., J., Wu., Y., Feng., X., Ma., Y., Huang., D., Li., Y., Dai., H., Fu., Q., and Huang., C.: An integrated source-profile dataset of high reactivity organic gases (HROG) for anthropogenic sources in China [dataset], https://doi.org/10.6084/m9.figshare.34948000, 2026.

Gkatzelis, G. I., Coggon, M. M., McDonald, B. C., Peischl, J., Aikin, K. C., Gilman, J. B., Trainer, M., and Warneke, C.: Identifying Volatile Chemical Product Tracer Compounds in U.S. Cities, Environ Sci Technol, 55, 188-199, 10.1021/acs.est.0c05467, 2021.

Guenther, A. B., Jiang, X., Heald, C. L., Sakulyanontvittaya, T., Duhl, T., Emmons, L. K., and Wang, X.: The Model of Emissions of Gases and Aerosols from Nature version 2.1 (MEGAN2.1): an extended and updated framework for modeling biogenic emissions, Geosci. Model Dev., 5, 1471-1492, 10.5194/gmd-5-1471-2012, 2012.

Hatch, L. E., Yokelson, R. J., Stockwell, C. E., Veres, P. R., Simpson, I. J., Blake, D. R., Orlando, J. J., and Barsanti, K. C.: Multi-instrument comparison and compilation of non-methane organic gas emissions from biomass burning and implications for smoke-derived secondary organic aerosol precursors, Atmos. Chem. Phys., 17, 1471-1489, 10.5194/acp-17-1471-2017, 2017.

Heald, C. L. and Kroll, J. H.: The fuel of atmospheric chemistry: Toward a complete description of reactive organic carbon, Science Advances, 6, 10.1126/sciadv.aay8967, 2020.

Huang, D. D., Hu, Q., He, X., Huang, R.-J., Ding, X., Ma, Y., Feng, X., Jing, S. a., Li, Y., Lu, J., Gao, Y., Chang, Y., Shi, X., Qian, C., Yan, C., Lou, S., Wang, H., and Huang, C.: Obscured Contribution of Oxygenated Intermediate-Volatility Organic Compounds to Secondary Organic Aerosol Formation from Gasoline Vehicle Emissions, Environ. Sci. Technol., 58, 10652-10663, 10.1021/acs.est.3c08536, 2024.

Huang, L., Zhao, B., Wang, S., Chang, X., Klimont, Z., Huang, G., Zheng, H., and Hao, J.: Global Anthropogenic Emissions of Full-Volatility Organic Compounds, Environ. Sci. Technol., 57, 16435-16445, 10.1021/acs.est.3c04106, 2023.

Koss, A. R., Sekimoto, K., Gilman, J. B., Selimovic, V., Coggon, M. M., Zarzana, K. J., Yuan, B., Lerner, B. M., Brown, S. S., Jimenez, J. L., Krechmer, J., Roberts, J. M., Warneke, C., Yokelson, R. J., and de Gouw, J.: Non-methane organic gas emissions from biomass burning: identification, quantification, and emission factors from PTR-ToF during the FIREX 2016 laboratory experiment, Atmos. Chem. Phys., 18, 3299-3319, 10.5194/acp-18-3299-2018, 2018.

Li, J., Xie, X., Li, L., Wang, X., Wang, H., Jing, S. a., Ying, Q., Qin, M., and Hu, J.: Fate of Oxygenated Volatile Organic Compounds in the Yangtze River Delta Region: Source Contributions and Impacts on the Atmospheric Oxidation Capacity, Environ. Sci. Technol., 56, 11212-11224, 10.1021/acs.est.2c00038, 2022a.

Li, M., Liu, H., Geng, G., Hong, C., Liu, F., Song, Y., Tong, D., Zheng, B., Cui, H., Man, H., Zhang, Q., and He, K.: Anthropogenic emission inventories in China: a review, National Science Review, 4, 834-866, 10.1093/nsr/nwx150, 2017a.

Li, M., Zhang, Q., Kurokawa, J.-i., Woo, J.-H., He, K., Lu, Z., Ohara, T., Song, Y., Streets, D. G., Carmichael, G. R., Cheng, Y., Hong, C., Huo, H., Jiang, X., Kang, S., Liu, F., Su, H., and Zheng, B.: MIX: a mosaic Asian anthropogenic emission inventory under the international collaboration framework of the MICS-Asia and HTAP, Atmos. Chem. Phys., 17, 935-963, 10.5194/acp-17-935-2017, 2017b.

Li, X., Qin, M., Li, L., Gong, K., Shen, H., Li, J., and Hu, J.: Examining the implications of photochemical indicators for O3–NOx–VOC sensitivity and control strategies: a case study in the Yangtze River Delta (YRD), China, Atmos. Chem. Phys., 22, 14799-14811, 10.5194/acp-22-14799-2022, 2022b.

Li, X., Li, X., Yan, R., Gao, Y., Gong, K., Wang, H., Qin, M., Hu, J., and Li, J.: Impact of primary oxygenated volatile organic compounds on ozone formation in the Yangtze River Delta region, Atmos. Chem. Phys., 26, 4901-4915, 10.5194/acp-26-4901-2026, 2026.

© Author(s) 2026. CC BY 4.0 License.



Liang, C. R., Feng, B. Y., Wang, S. X., Zhao, B., Xie, J. Z., Huang, G. H., Zhu, L., and Hao, J. M.: Differentiated emissions and secondary organic aerosol formation potential of organic vapor from industrial coatings in China, Journal of Hazardous Materials, 466, 10.1016/j.jhazmat.2024.133668, 2024.

Lu, J., Gao, Y., Huang, D., Jing, S. a., Wang, H., Li, Y., Ding, X., Hu, Q., Xiu, G., Lin, M., Zhang, W., and Huang, C.: Reactive Organic Gases from Vehicle Evaporative Emissions: Rates, Compositions, and Temperature Effects, Environ. Sci. Technol., 59, 11132-11144, 10.1021/acs.est.4c09415, 2025.

Lyu, X., Li, H., Lee, S.-C., Xiong, E., Guo, H., Wang, T., and de Gouw, J.: Significant Biogenic Source of Oxygenated Volatile Organic Compounds and the Impacts on Photochemistry at a Regional Background Site in South China, Environ. Sci. Technol., 58, 20081-20090, 10.1021/acs.est.4c05656, 2024.

Ministry of Ecology and Environment of China: Technical Guide for Compiling Integrated Emission Inventory of Air Pollutants and Greenhouse Gases (Trial), 2024.

Ministry of Ecology and Environment of the People's Republic of China: Ambient air-Determination of aldehyde and ketone compounds-High performance liquid chromatography, 2014.

Ministry of Ecology and Environment of the People's Republic of China: Specifications and Test Procedures for Ambient Air Quality Continuous Monitoring System with Gas Chromatography for Volatile Organic Compounds, 2018.

Ministry of Ecology and Environment of the People's Republic of China: Standard for fugitive emission of volatile organic compounds, 2019.

Mo, Z., Shao, M., and Lu, S.: Compilation of a source profile database for hydrocarbon and OVOC emissions in China, Atmos. Environ., 143, 209-217, 10.1016/j.atmosenv.2016.08.025, 2016.

Pagonis, D., Sekimoto, K., and de Gouw, J.: A Library of Proton-Transfer Reactions of H3O(+) Ions Used for Trace Gas Detection, J Am Soc Mass Spectrom, 30, 1330-1335, 10.1007/s13361-019-02209-3, 2019.

Qin, M., She, Y., Wang, M., Wang, H., Chang, Y., Tan, Z., An, J., Huang, J., Yuan, Z., Lu, J., Wang, Q., Liu, C., Liu, Z., Xie, X., Li, J., Liao, H., Pye, H. O. T., Huang, C., Guo, S., Hu, M., Zhang, Y., Jacob, D. J., and Hu, J.: Increased urban ozone in heatwaves due to temperature-induced emissions of anthropogenic volatile organic compounds, Nature Geoscience, 18, 50-56, 10.1038/s41561-024-01608-w, 2025.

Sekimoto, K., Li, S.-M., Yuan, B., Koss, A., Coggon, M., Warneke, C., and de Gouw, J.: Calculation of the sensitivity of proton-transfer-reaction mass spectrometry (PTR-MS) for organic trace gases using molecular properties, International Journal of Mass Spectrometry, 421, 71-94, 10.1016/j.ijms.2017.04.006, 2017.

Sha, Q. e., Zhu, M., Huang, H., Wang, Y., Huang, Z., Zhang, X., Tang, M., Lu, M., Chen, C., Shi, B., Chen, Z., Wu, L., Zhong, Z., Li, C., Xu, Y., Yu, F., Jia, G., Liao, S., Cui, X., Liu, J., and Zheng, J.: A newly integrated dataset of volatile organic compounds (VOCs) source profiles and implications for the future development of VOCs profiles in China, Sci Total Environ, 793, 148348, https://doi.org/10.1016/j.scitotenv.2021.148348, 2021.

Simon, H., Beck, L., Bhave, P. V., Divita, F., Hsu, Y., Luecken, D., Mobley, J. D., Pouliot, G. A., Reff, A., Sarwar, G., and Strum, M.: The development and uses of EPA's SPECIATE database, Atmospheric Pollution Research, 1, 196-206, https://doi.org/10.5094/APR.2010.026, 2010.

Stockwell, C. E., Coggon, M. M., Gkatzelis, G. I., Ortega, J., McDonald, B. C., Peischl, J., Aikin, K., Gilman, J. B., Trainer, M., and Warneke, C.: Volatile organic compound emissions from solvent- and water-borne coatings - compositional differences and tracer compound identifications, Atmos. Chem. Phys., 21, 6005-6022, 10.5194/acp-21-6005-2021, 2021.

Tanzer-Gruener, R., Rajan, P. E., Dugan, L. D., Bier, M. E., Robinson, A. L., and Presto, A. A.: Watching Paint Dry: Organic Vapor Emissions from Architectural Coatings and their Impact on Secondary Organic Aerosol Formation, Environ. Sci. Technol., 10.1021/acs.est.2c02478, 2022.

Wang, S., Yuan, B., Wu, C., Wang, C., Li, T., He, X., Huangfu, Y., Qi, J., Li, X. B., Sha, Q., Zhu, M., Lou, S., Wang, H., Karl, T., Graus, M., Yuan, Z., and Shao, M.: Oxygenated volatile organic compounds (VOCs) as significant but varied contributors to VOC emissions from vehicles, Atmos. Chem. Phys., 22, 9703-9720, 10.5194/acp-22-9703-2022, 2022a.

Wang, W., Yuan, B., Peng, Y., Su, H., Cheng, Y., Yang, S., Wu, C., Qi, J., Bao, F., Huangfu, Y., Wang, C., Ye, C., Wang, Z., Wang, B., Wang, X., Song, W., Hu, W., Cheng, P., Zhu, M., Zheng, J., and Shao, M.: Direct observations indicate photodegradable oxygenated volatile organic compounds (OVOCs) as larger contributors to radicals and ozone production in the atmosphere, Atmos. Chem. Phys., 22, 4117-4128, 10.5194/acp-22-4117-2022, 2022b.

Xiong, E., Guo, H., Fu, T.-M., Lyu, X., Wang, Y., Zhou, B., Xia, M., Zou, Z., Yuan, Q., Yang, J., Shek, K. Y., Chen, J., Jiang, T., Tao, W., Zhang, A., Xiang, W., Lee, S., and Wang, T.: OVOCs drive radical cycling and ozone formation in background air, Environmental Science and Ecotechnology, 29, 100659, https://doi.org/10.1016/j.ese.2026.100659, 2026.

Yan, R., Wang, H., Huang, C., An, J., Bai, H., Wang, Q., Gao, Y., Jing, S., Wang, Y., and Su, H.: Impact of spatial scales of control measures on the effectiveness of ozone pollution mitigation in eastern China, Sci Total Environ, 906, 167521, 10.1016/j.scitotenv.2023.167521, 2024.

Zheng, B., Tong, D., Li, M., Liu, F., Hong, C., Geng, G., Li, H., Li, X., Peng, L., Qi, J., Yan, L., Zhang, Y., Zhao, H., Zheng, Y., He, K., and Zhang, Q.: Trends in China's anthropogenic emissions since 2010 as the consequence of clean air actions, Atmos. Chem. Phys., 18, 14095-14111, 10.5194/acp-18-14095-2018, 2018.